Journal of Magnetism and Magnetic Materials 74 (1988) 158–164
North-Holland, Amsterdam

THE MAGNETIC STRUCTURE OF $NaMnFeF_6$

G. COURBION and M. LEBLANC

Laboratoire des Fluorures, UA 449, Université du Maine, 72017 Le Mans Cedex, France

Received 10 April 1988

The "spin mou" behaviour of $NaMnFeF_6$ is studied by neutron diffraction below T_c (45 K). The magnetic structure results from an antiferromagnetic coupling between Fe(1a), Fe(2d) and Mn(3f) sublattices. The magnetic moments (μ(Fe1a) = $-4.34\mu_B$, μ(Fe2d) = $-4.42\mu_B$, μMn(3f) = $4.70\mu_B$ at $T = 2$ K) are collinear with the c axis of the trigonal cell (S.G. P321, $Z = 3$, $a = 9.021(2)$ Å, $c = 4.962(1)$ Å at $T = 2$ K). The Fe(2d) sublattice is weakly coupled to the net magnetization at $T > 2$ K; this behaviour is related to an edge sharing octahedral geometry. A comparison with isotypic $LiMnFeF_6$ compounds is given.

1. Introduction

Among the ternary fluorides $AMM'F_6$ of the Na_2SiF_6-type, β-$LiMnFeF_6$ [1] and $NaMnFeF_6$ [2,3] exhibit a peculiar magnetic behaviour referenced as "spin fou" and "spin mou", respectively. These phases have trigonal symmetry (space group: P321, $Z = 3$) and the magnetic properties are strongly dependent on the cationic distribution in the crystallographic sites 1a, 2d, 3e and 3f.

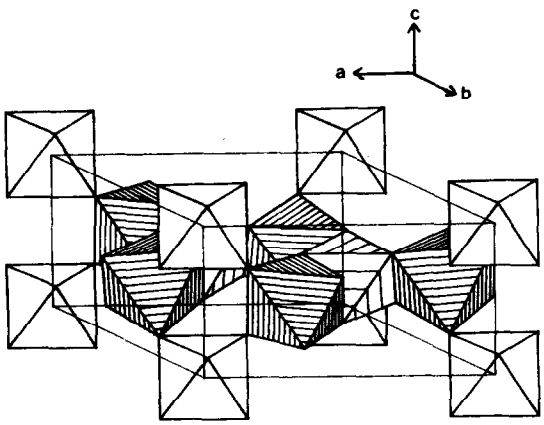

Fig. 1. Representation of the paramagnetic network of $NaMnFeF_6$ (Mn, Fe(2d) and Fe(1a) octahedra are respectively symbolised with strong, slight and no hatching).

$NaMnFeF_6$ ($a = 9.041(2)$ Å, $c = 5.004(2)$ Å at room temperature) is isotypic with the $NaMnCrF_6$ structure [4]. The paramagnetic octahedra network, with Fe^{3+} in 1a and 2d and Mn^{2+} in 3f, is shown in fig. 1. At $z = 1/2$, each Fe(2d) octahedron shares an edge with three Mn(3f) octahedra and the resulting layers – $Mn_3Fe_2F_{18}$ – are connected one to each other by Fe(1a) octahedra. Magnetic measurements and Mössbauer spectroscopy [2] evidence a ferrimagnetic behaviour. Below $T_c = 45$ K, the thermal variation of the hyperfine field at Fe(1a) and Fe(2d) sites is different and the remanent magnetization peaks at 32 K (see fig. 4b).

The present work is devoted to the determination of the magnetic structure of $NaMnFeF_6$ at temperatures between 45 and 2 K by using neutron diffraction experiments.

2. Experimental details

$NaMnFeF_6$ is a metastable phase and is only prepared at low temperature by hydrothermal synthesis [5]. The obtainment of large amounts of compound requires the use of a Paar bomb for acid digestion with a teflon cup in the following conditions: 6.5 g of powder ($NaF/MnF_2/FeF_3$;

1/1/1), 5 ml aqueous HF 48%, two days at 220 °C ($P \approx 220$ bar) and slow cooling to room temperature. The resulting light pink powder of $NaMnFeF_6$ is slightly contaminated with a small amount of $MnFeF_5 \cdot 2H_2O$ [6] (removed by hand) and MnF_2.

Powder neutron diffraction spectra were recorded at the Institut Laue Langevin in Grenoble with the D1B high resolution powder diffractometer ($18° < 2\theta < 98°$ in steps of 0.2°, $\lambda = 2.52$ Å) in the temperature range 2–60 K. After data reduction, the magnetic and/or nuclear structures

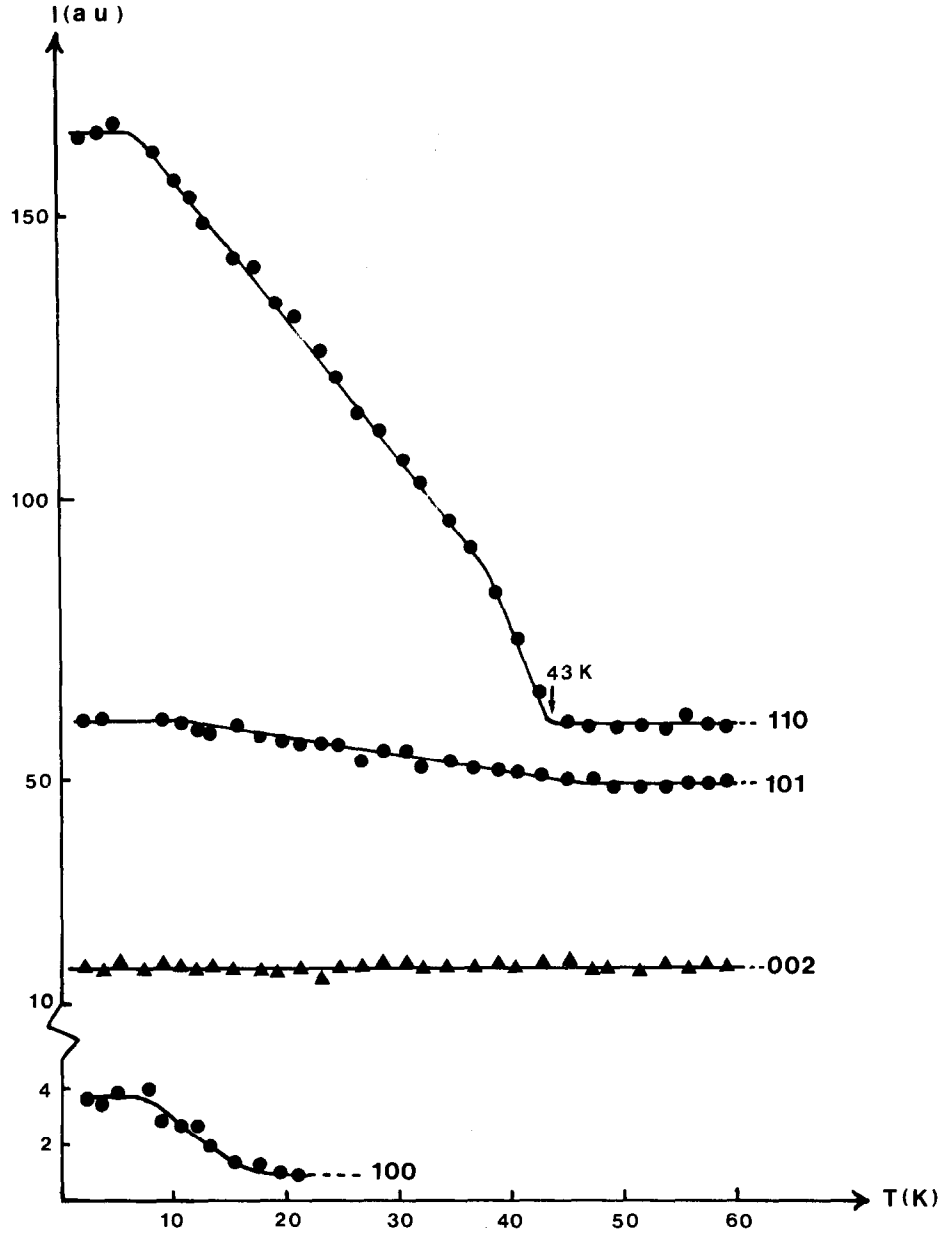

Fig. 2. Thermal variation of the intensities of selected reflections.

were refined by the Rietveld method [7,8]. Neutron scattering lengths and magnetic form factors were taken from refs. [9] and [10], respectively.

Table 1
Atomic coordinates of $NaMnFeF_6$ at $T = 50$ K ($a = 9.017(2)$ Å, $c = 4.966(1)$ Å)

Atom	Site	x	y	z	B (Å^2) [a]
Na	3e	0.373(3)	0	0	0.1
Mn	3f	0.711(3)	0	1/2	0.1
Fe	1a	0	0	0	0.1
Fe	2d	1/3	2/3	0.511(1)	0.2
F_1	6g	0.899(3)	0.102(2)	0.776(3)	0.2
F_2	6g	0.535(2)	0.404(2)	0.712(3)	0.2
F_3	6g	0.231(2)	0.770(3)	0.706(3)	0.2

[a] Fixed; esd's are given in parentheses and refer to the last digit.

Table 2
Average distances and angles of $NaMnFeF_6$ ($T = 50$ K)

M–F (Å)	Mn–F–Fe (°)	Mn–Fe (Å)
Na: 2.33	Fe2d:102	3.22
Mn: 2.11	107	3.22
Fe1a: 1.94	Fe1a:132	3.60
Fe2d: 1.91		

3. Neutron diffraction study

Neutron diffraction patterns at 2, 15, 27, 34, 38 and 50 K were selected for line profile analysis. Below T_c, the magnetic cell and the nuclear cell are identical. The thermal variation of the integrated intensity of several reflections is given in fig. 2. The main magnetic contribution appears on the (110) line and the nuclear level is recovered

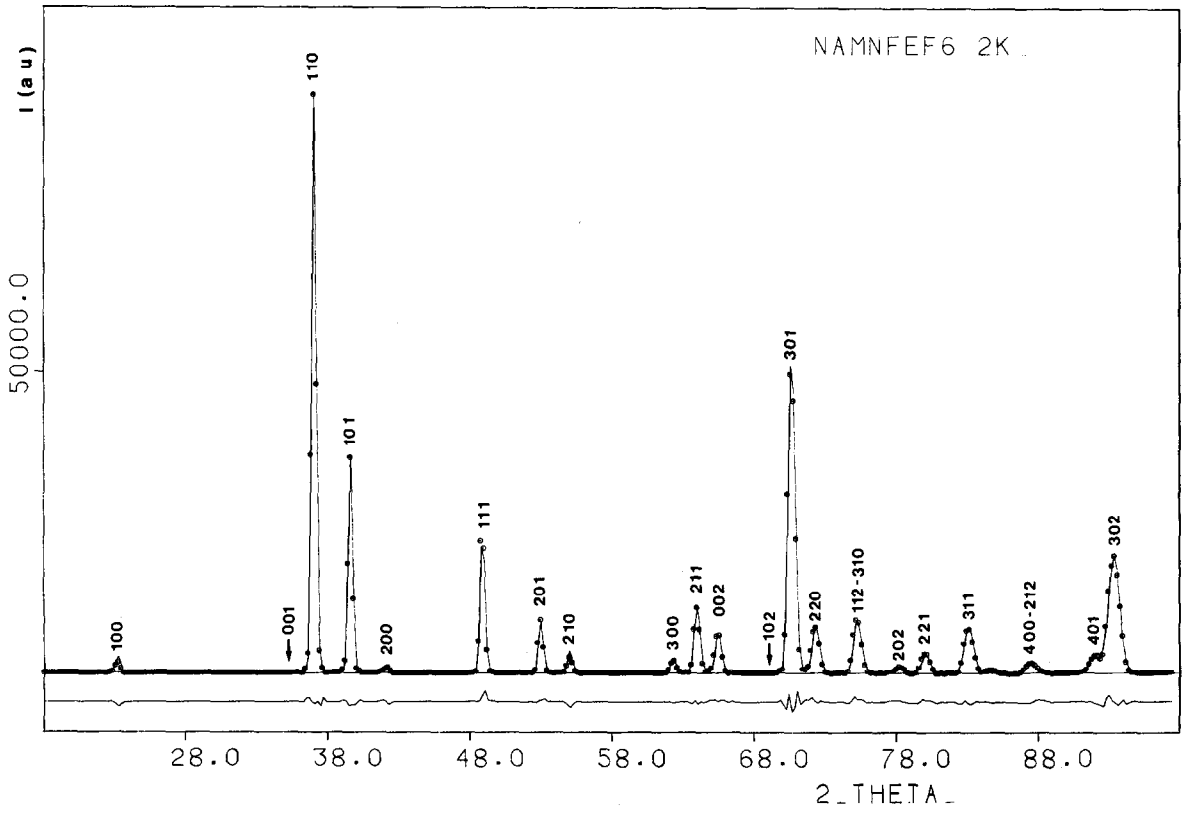

Fig. 3. Neutron diffraction pattern at 2 K (○: observed, −; calculated and difference patterns. (001) and (102) lines are rejected because they are in the vicinity of MnF_2 (001)mag and (111) lines, respectively).

around 43 K with exception of the (100) line ($\approx$ 20 K). Furthermore, the absence of any magnetic contribution on the (001) and (002) lines suggests a collinear ferrimagnetic model along the c direction.

The profile refinement of the 50 K nuclear

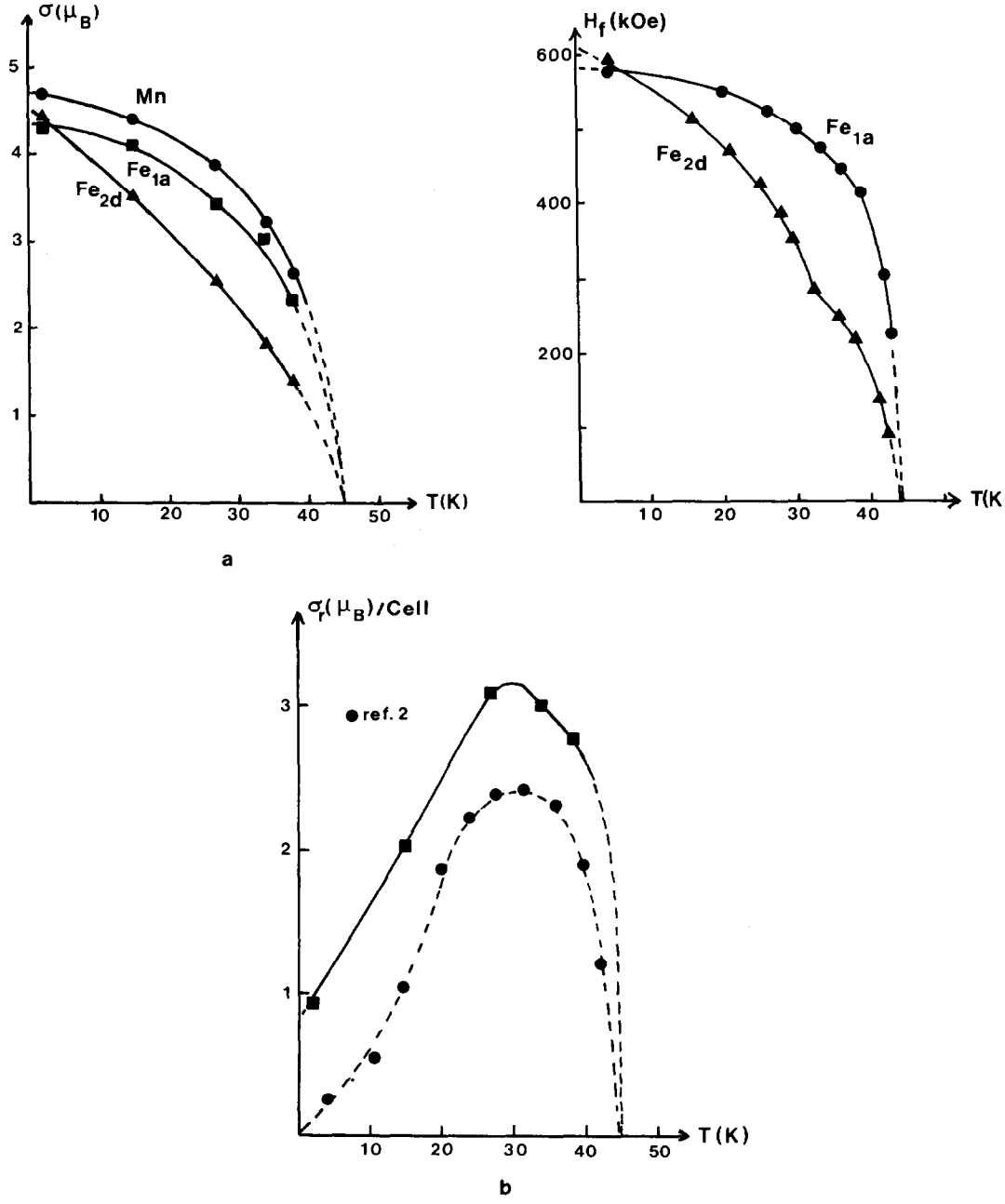

Fig. 4. (a) Thermal variation of the magnetic moment of Mn(3f), Fe(2d) and Fe(1a) (left) compared to the hyperfine fields at Fe(1a) and Fe(2d) (taken from ref. [2]) (right); (b) thermal variation of the calculated (■) and measured (●) (from ref. [2]) ferrimagnetic component.

Table 3
Magnetic moments, remanent magnetization and discrepancy factors from Rietveld profile refinements

	$T = 2K$	15 K	27 K	34 K	38 K
* Mn(3f)	4.70(11)	4.42(14)	3.87(14)	3.22(15)	2.64(15)
* Fe(2d)	−4.42(13)	−3.57(17)	−2.54(18)	−1.18(20)	−1.40(21)
* Fe(1a)	−4.34(11)	−4.10(6)	−3.42(18)	−3.06(23)	−2.35(17)
$*\sigma_r$	0.92	2.02	3.11	2.98	2.77
R_P	0.0681	0.0960	0.0864	0.0913	0.0954
R_I	0.0325	0.0650	0.0453	0.0519	0.0504
R_{nucl}	0.0279	0.0590	0.0414	0.0475	0.0487
R_{mag}	0.0407	0.0783	0.0582	0.0735	0.0626

σ_r is given for one unit cell (* unit: μ_B) – esd's are given in parentheses.

pattern ($R_I = 0.026$, $R_P = 0.072$) leads to the atomic coordinates given in table 1. The average distances (table 2) are in good agreement with the sum of ionic radii [11] and the average angles are close to those observed for isotypic compounds: the Fe–F–Mn angles in edge and corner sharing octahedra lie around 100° and 132°, respectively. The atomic coordinates were kept at their 50 K values during the refinement of the low temperature patterns.

From the basis vectors of the representation analysis method of Bertaut previously described in section 3.2.2 of ref. [1], only the Γ_2 magnetic mode (F_z for each sublattice) allows to fit the observed intensities (fig. 3). Within the accuracy of the experiments, a collinear model with spins along the c axis can be proposed with the following combination of signs: Mn(3f) +, Fe(2d) − and Fe(1a) −; the results of the profile refinements are given in table 3. The thermal variation of the sublattice magnetization and of the deduced ferrimagnetic component is shown in fig. 4a and b, respectively; they are in good agreement with the Mössbauer and magnetization experiments.

4. Discussion

The model suggested by the neutron diffraction study is illustrated in fig. 5. Antiferromagnetic interactions between Fe(1a) and six Mn(3f) neighbours and between Fe(2d) and three Mn(3f) neighbours occur via 132° or 100° superexchange pathways, respectively. From fig. 4a, it can be seen that Mn(3f) and Fe(1a) moments have a quite similar thermal dependence whereas the decrease of Fe(2d) moment is faster. This weak Fe(2d) coupling to the Net magnetization is accountable for the ferrimagnetic component variation which shows a maximum around 30 K (fig. 4b). These results are well explained if d^5–d^5 superexchange interactions at 100° (edge sharing) are weaker than d^5–d^5 interactions at 132° (corner sharing) as expected from Kanamori–Goodenough rules [12,13]. This was analysed by Lacorre from a Monte Carlo simulation [14]: the adjusted coupling constants, $J_{132°}$ (Mn–Fe(1a)) = −3 K and $J_{100°}$ (Mn–Fe(2d)) = −0.5 K, allow to explain the "spin mou" behaviour without any change of the magnetic structure between 2 and 45 K.

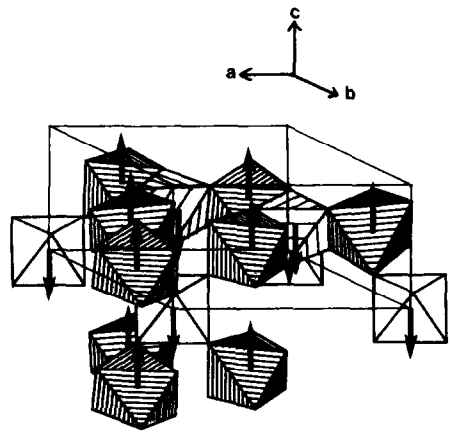

Fig. 5. Magnetic structure of $NaMnFeF_6$ (for sake of clarity the Fe(1a) octahedra at $z = 1$ have been omitted).

Table 4
Site occupancy, magnetic environment and magnetic order temperatures in $AMnFeF_6$ compounds

α-$LiMnFeF_6$ antiferromagnet	1Mn(3e) → 6Fe(3f)–132° –	1Fe(3f) → 6Mn(3e)–132° –	$T = 158$ K
β-$LiMnFeF_6$ ferrimagnet	1Mn(3e) → 4Fe(2d)–132° –	1Fe(2d) → 6Mn(3e)–132° –	$T = 115$ K
	→ 1Fe(1a)–100° –	1Fe(1a) → 3Mn(3e)–100° –	$T = 2$ K
	"spin fou"		
$NaMnFeF_6$ ferrimagnet	1Mn(3f) → 2Fe(1a)–132° –	1Fe(1a) → 6Mn(3f)–132° –	$T = 45$ K
	→ 2Fe(2d)–100° –	1Fe(2d) → 3Mn(3f)–100° –	$T = 45$ K
	"spin mou"		

The arrows indicate "is surrounded by".

Such an anomaly of the magnetization of the iron sites, in edge sharing octahedral geometry, was encountered with β-$LiMnFeF_6$ for the Fe(1a) site (fig. 6a). This compound and its low temperature variety α-$LiMnFeF_6$ are also related to the Na_2SiF_6 structure [1] with similar superexchange angles but with different cationic orders. Table 4 summarizes the characteristics of the three $AMnFeF_6$ phases: the site occupancy for manganese and iron cations, the number of first neighbours for each manganese and iron with the corresponding superexchange angles and the magnetic ordering temperatures. Some remarks arise from this table:

1) Magnetic superexchange interactions at 132° and 100° are always antiferromagnetic.

2) The different cationic ordering in the three structures leads to a modification of the number of Fe^{3+} cations around one Mn^{2+} cation: 6, 5 and 4 for α-$LiMnFeF_6$, β-$LiMnFeF_6$ and $NaMnFeF_6$, respectively.

3) Whatever the cationic order, no anomaly is observed in the magnetization of Fe^{3+} sites when they are surrounded by six Mn^{2+} with strong antiferromagnetic interactions at 132°.

4) The anomalies always occur on the Fe^{3+} sites surrounded by three Mn^{2+} (fig. 6a and b) with weak antiferromagnetic interactions at 100°: Fe(1a) in α-$LiMnFeF_6$ presents a "spin fou" behaviour (Fe(1a) remains paramagnetic down to 2 K whereas Mn(3e) and Fe(2d) order magnetically at 115 K) and Fe(2d) in $NaMnFeF_6$ has a "spin mou" behaviour. The main difference between both compounds concerns the connection mode of the (Mn_3Fe) units in the (a, b) plane: isolated in β-$LiMnFeF_6$ and connected by a common manganese octahedron in $NaMnFeF_6$.

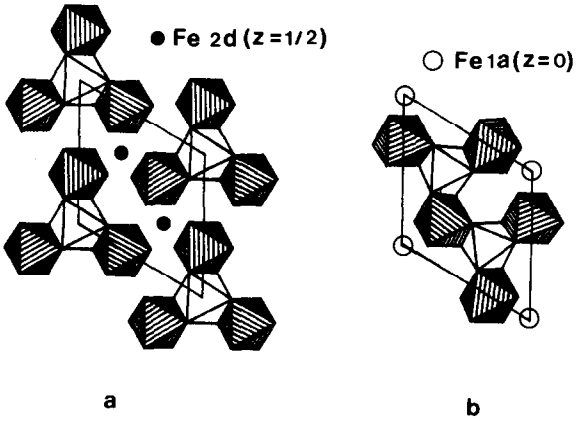

Fig. 6. (001) projection at $z = 0$ and $z = 1/2$ levels of β-$LiMnFeF_6$ (a) and $NaMnFeF_6$ (b), respectively.

5. Conclusion

The magnetic structure of $NaMnFeF_6$ is solved at five temperatures between 2 and 45 K. Strong antiferromagnetic coupling arises between Mn(3f) and Fe(2d) at 132° superexchange angles. The magnetization at Fe(2d) site ("spin mou" behaviour) decreases faster than the magnetization at Mn(3f) and Fe(1a) sites and is responsible for the observed ferrimagnetism. As for β-$LiMnFeF_6$, the ferrimagnetic properties of $NaMnFeF_6$ are related to a weak d^5–d^5 antiferromagnetic coupling between FeF_6 and MnF_6 octahedra sharing edges with a superexchange angle close to 100°.

Acknowledgements

The authors gratefully acknowledge Dr. J. Pannetier for help in data collection and Professor G. Ferey for helpful discussions.

References

[1] G. Courbion, R. De Pape, J. Teillet, F. Varret and J. Pannetier, J. Magn. Magn. Mat. 42 (1984) 217.
[2] M. Tamine, Y. Calage, M. Leblanc, G. Ferey and F. Varret, Hyperfine Interactions 28 (1986) 529.
[3] M. Tamine and Y. Calage, J. Phys. Chem. Solids 48 (1987) 1235.
[4] G. Courbion, C. Jacoboni and R. De Pape, Acta Cryst. B33 (1977) 1405.
[5] M. Leblanc, Thèse d'Etat, Le Mans (1984).
[6] Y. Laligant, J. Pannetier, M. Leblanc, P. Labbe, G. Heger and G. Ferey, Z. Krist. (in press).
[7] H.M. Rietveld, J. Appl. Cryst. 2 (1969) 65.
[8] A.W. Hewat, Harwell Report AERE-R 7350 (1973).
[9] L. Koester and H. Rauch, IAEA Contract 2517/RB (1981).
[10] R.E. Watson and A.J. Freeman, Acta Cryst. 14 (1961) 27.
[11] R.D. Shannon, Acta Cryst. A 32 (1976) 751.
[12] J. Kanamori, J. Phys. Chem. Solids 10 (1959) 87.
[13] J.B. Goodenough, in: Magnetism and the Chemical Bond (Interscience–John Wiley, New York, 1963).
[14] P. Lacorre and J. Pannetier, J. Magn. Magn. Mat. 71 (1987) 63.